Labile Ferroelastic Nanodomains in Bilayered Ferroelectric Thin Films

By *Varatharajan Anbusathaiah,* Daisuke Kan, Fransiska C. Kartawidjaja, Reza Mahjoub, Miryam A. Arredondo, Samantha Wicks, Ichiro Takeuchi, John Wang,* and *Valanoor Nagarajan**

Heterostructured thin films differing either in their structure, composition, or in both have shown novel magnetic,[1,2] superconducting,[3] ferroelectric, or electromechanical[4,5] responses. In the case of ferroelectrics, multilayers or superlattices have displayed enhanced polarization,[5–7] high dielectric permittivity[8,9] and in some instances, entirely new structural phases.[10] These observations have been accounted for on the basis of electric-field-induced coupling,[4] epitaxial strain,[11,12] and specific polar interactions between the interfacial layers.[5,10,13,14] As most ferroelectrics have a strong non-negligible ferroelastic self-strain associated with their phase transformation, an aspect that should be equally fascinating is that of the elastic interactions between such multilayers. The interactions lead to the formation of ferroelastic domains, arranged in the form of period-alternating lamellae in order to relax the excess elastic energy. When these lamellae are of the same phase but of different crystallographic orientations, they are generally referred to as ''twins''. The ferroelastic-domain-wall (extrinsic) contribution to the dielectric, piezoelectric, and elastic properties of ferroelectrics is indeed quite significant[15] in the case of bulk ceramics and single-crystals, and this can be several times larger than the intrinsic lattice piezoresponse.[16]

In the case of ferroelectric thin films, the issue of movement of ferroelastic domains is not without debate. Earlier experimental studies[17,18] proposed that the ferroelastic ''herringbone'' pattern in thin films demonstrated very limited (if any) ability to move under external stress or electric field. This has been contradicted in more recent experiments on polycrystalline films.[19,20] Nevertheless, gross quantitative enhancement has been reported only under special conditions, such as films patterned into islands,[21] under nonuniform electric field,[22] or on specially orientated substrates (such as (101) $SrTiO_3$).[23]

In this communication, we demonstrate that a bilayered heterostructure, comprised of a tetragonal (T) $PbZr_{0.3}Ti_{0.7}O_3$ film deposited on a rhombohedral (R) $PbZr_{0.7}Ti_{0.3}O_3$ film, on electrode-buffered Si substrates leads to a nanoscale ferroelastic-domain arrangement that is easily susceptible to external electric fields. Piezoresponse force microscopy (PFM) and cross-sectional transmission electron microscopy (TEM) analyses of these layered structures show complex ferroelastic-domain arrangement to be present only in the Ti-rich top tetragonal layer. Thus, these domains are tethered only by a soft Zr-rich R underlayer, and not by the hard substrate. They move under the application of an external electric field leading to a giant piezoelectric coefficient of $\approx$220 pm V^{-1}, up to three times larger than what is normally observed in constrained single-layered PZT thin films. X-ray diffraction (XRD) patterns taken following applications of an electric field reveal a distinct change in the ferroelastic (non-180°)-domain population distribution. Most importantly, we find that this motion in a simple thin-film geometry is reversible and repeatable with cyclic application of electric fields. Such ferroelastic-domain motion is very attractive for a variety of electromechanical devices.

Figure 1 is a panel showing a series of PFM images and the cross-sectional TEM image obtained for a 70 nm thick $PbZr_{0.3}Ti_{0.7}O_3$ (T)/70 nm thick $PbZr_{0.7}Ti_{0.3}O_3$ (R) bilayer on a $Pt/Ti/SiO_2/Si$ substrate. Figure 1a shows the out-of-plane $R\cos\theta$ (Vertical PFM or VPFM) image. The dotted lines in this image represent the grain boundaries traced from the topography (in Supporting Information), which reveal a relatively large grain size (1–3 μm) for such a thin film.

Arlt[24] has previously analyzed how 3D-configured ferroelastic domains are accommodated in bulk ceramics, and concluded that complex self-assembled domains could not be formed unless the material had a very large grain size (several square micrometers). This emphasizes the critical role of the large grain size in our bilayered films, which provides the fundamental requirement to form complex nanodomain hierarchies. The corresponding in-plane piezoresponse-force image (Lateral PFM or LPFM) captured simultaneously (Fig. 1b) clearly shows the varying domain arrangements within each grain. The bright (white) and the dark (blue) contrast in out-of-plane and in-plane PFM images represent the direction of orientation of the polarization vector in their respective planes. Regions that show a strong signal in the in-plane PFM image show a poor signal (orange contrast) in the corresponding out-of-plane image, thus implying that these are the ''*a*-domain'' fractions in these bilayered thin films. A rough

[*] V. Anbusathaiah, Dr. V. Nagarajan, R. Mahjoub, M. A. Arredondo, S. Wicks
School of Materials Science & Engineering
University of New South Wales
Sydney, NSW 2052 (Australia)
E-mail: anbu@materials.unsw.edu.au; nagarajan@unsw.edu.au
F. C. Kartawidjaja, Prof. J. Wang
Department of Materials Science and Engineering
National University of Singapore
Singapore, 117576 (Singapore)
Dr. D. Kan, Prof. I. Takeuchi
Department of Materials Science and Engineering
University of Maryland
College Park, MD 20742 (USA)

DOI: 10.1002/adma.200803701

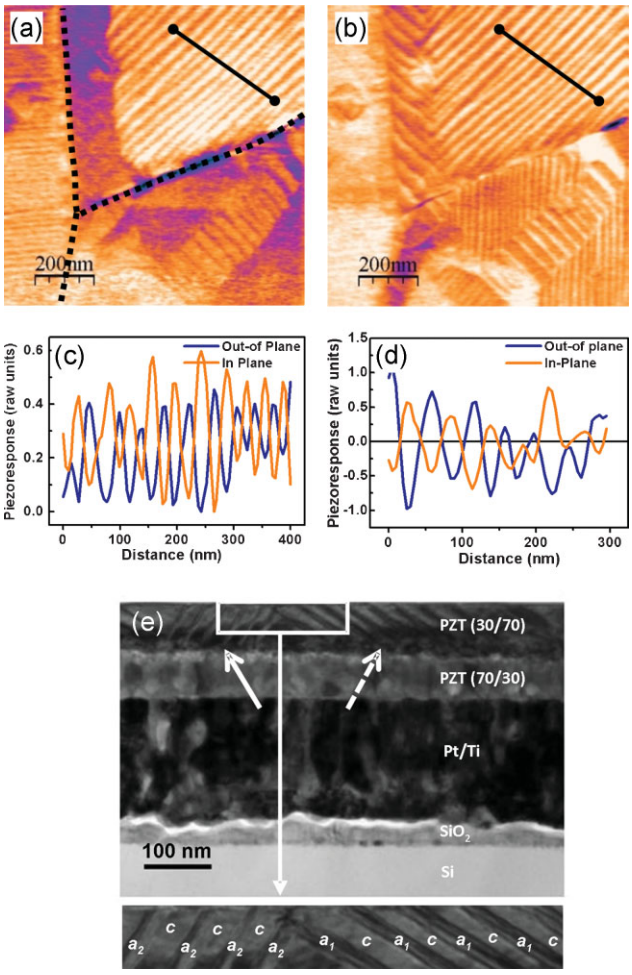

Figure 1. Twinned ferroelastic-domain structure for the bilayered PZT thin films. a) Vertical PFM image with dotted line representing the grain boundaries. b) Corresponding lateral PFM image. c) Cross-sectional profile for the line shown in the VPFM and LPFM images. d) Similar cross-sectional profile drawn for an alternative domain pattern. e) Cross-sectional TEM image of the bilayered PZT thin films that reveals the twin domain structure for the top T surface. The bottom inset is the magnified portion that shows $c/a_1/c/a_1$ and $c/a_2/c/a_2$ domain structures.

estimate from this visual image leads to a ferroelastic twin fraction of more than 50%, normally unexpected for this composition and especially at such small film thicknesses.[25] This is also seen in the $\theta - 2\theta$ XRD scans (in Supporting Information), which revealed the presence of a significant *a*-domain fraction. The PFM images show fine domain twinning throughout the entire film, and although the periodicities of these domains vary from grain to grain and from region to region, the pattern is overall unlike the square-grid-type structures previously observed in epitaxial PZT.[17,22] Instead, the PFM images bear a strong resemblance to the stripe or lamellar arrangement demonstrated recently for single-crystal $BaTiO_3$ nanowires,[26] thus implying a domain state significantly distinct from commensurate single-layered thin films. Indeed, single-layered films of equivalent thicknesses did not display such complex domain arrangements or grain sizes (shown in Supporting Information).

To identify the domain configurations, we look at cross-sectional profiles from the VPFM and LPFM images. Figure 1c represents one such profile along the black line in Figure 1a and b. It shows that both the out-of-plane and in-plane components have the same magnitude but are in opposite phases spatially, that is, the maxima of the out-of-plane magnitude coincide with the minima of the in-plane magnitude, and vice-versa. In other words, a given domain has either out-of-plane component (*c*-domain) or in-plane (*a*-domain) component but never both. This is the classic case of $c/a/c/a$ domain structures with (001)/(100) orientation, following the 3D analyses of the PFM images by Eng and Ganpule et al.[17,27] A second case is the cross-sectional profile shown in Figure 1d, obtained from a different grain (not shown here) in the same thin film. In this case, the maxima and minima for the out-of-plane and in-plane piezoresponse are coincident along the spatial direction, indicating that for this domain both in-plane and out-of-plane signals exist, and thus from vector-PFM analysis[28] the polarization is at an angle to the substrate normal. The X-ray diffraction for this bilayered structure showed that other than (100)/(001) grains, (111) and (110) orientations also exist. We thus believe Figure 1d is from a (111) or (101) oriented grain. A cross-sectional TEM image (Fig. 1e) confirms the presence of several $c/a/c/a$ domain configurations within a single grain. We note that the twin domains are present only in the top Ti-rich T layer. The bottom Zr-rich R layer is totally devoid of any form of twinning or ferroelastic domains. Further, it also shows the different possible $c/a/c/a$ domain types, with the boxed inset in Figure 1e magnified to render a clearer image of the varying ferroelastic domain arrangements with different angles of orientations (denoted by arrows).

Figure 2 is a panel showing the PFM domain-imaging result of switching experiments performed within one large grain. The left-column images show the VPFM and the right column show the LPFM images (both are R cosθ images). Figure 2a and b show the as-grown domain state, 2c and d are the images after the application of DC bias (-5 V) at the center (500 nm $\times$ 500 nm), and Figure 2e and f are the VPFM and LPFM images after $+5$ V DC bias on the same region, respectively. First, the cross-sectional profile (inset to Fig. 2c) of the VPFM image confirms a change in sign of the phase of the VPFM signal going from the unwritten region to inside the written square. This proves that the change in contrast is a true domain-switching effect rather than a simple surface-charge-induced effect. Interestingly, under applied electric field, only the top diagonal region becomes bright, whereas the bottom left diagonal of the region switches to the opposite phase (dark contrast) with a significant domain reconstruction, as marked by the arrow. The corresponding LPFM image shows that the in-plane-oriented *a*-domains have also switched to give bright contrast with twin reconstruction, which is a clear indication of 90° ferroelastic-domain-wall movement. In Figure 2e and f (after positive bias) the nanodomains relax back to the original position in the top-right diagonal, whereas in the bottom left diagonal they break down into many more $c/a/c/a$ nanodomain patterns.

To probe if the changes in the domain patterns are due to an electric-field-induced phase transition (as postulated by Fu et al.[29] and Bellaiche et al.[30]), we have studied the effect of electric field on the X-ray-diffraction (XRD) pattern of the film

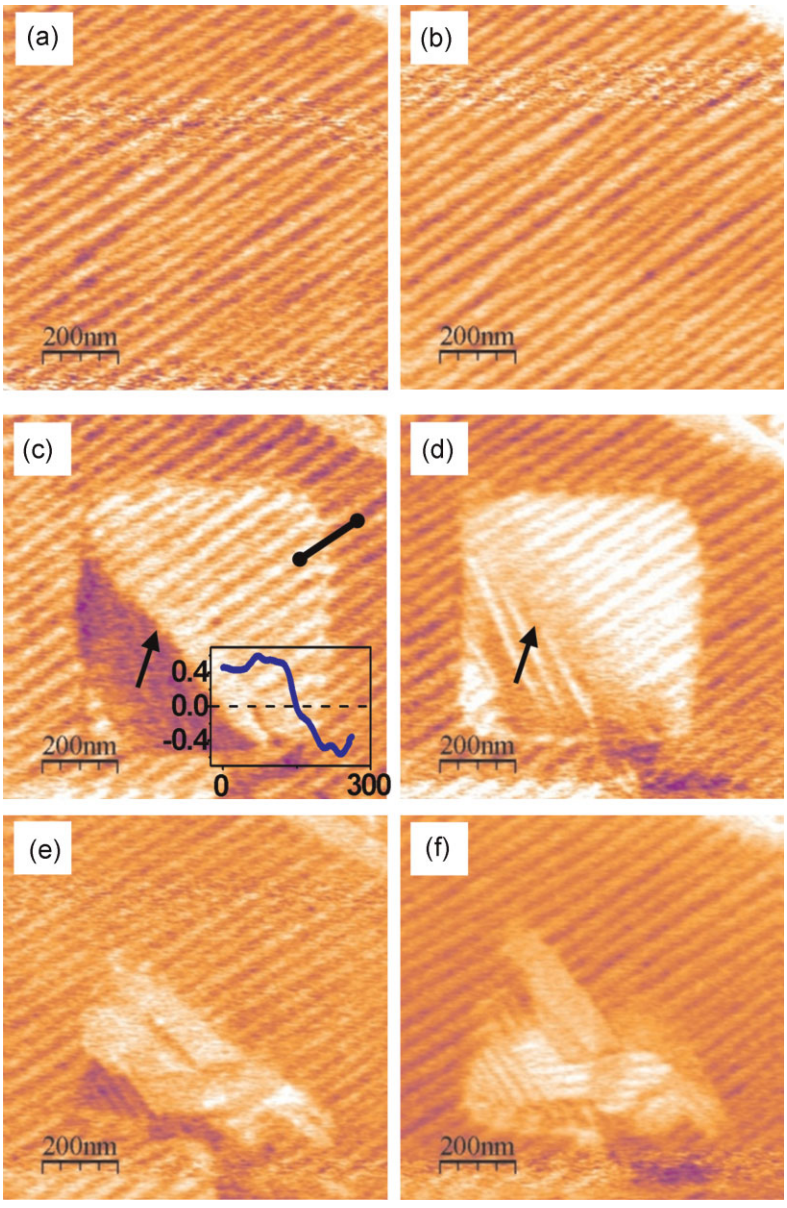

Figure 2. PFM images that demonstrate 90° domain switching in bilayered thin films. a) VPFM image before applying DC bias. b) Corresponding LPFM image. c,d) VPFM and LPFM images after applying −5 V DC bias. Inset represents the cross-section profile for the line marked in c). Arrows in this figures point the domain rearrangements. e,f) VPFM and LPFM images after applying +5 V DC bias.

using a lab diffractometer (Bruker D8). The smallest possible spot size for the X-ray beam was ≈3 mm^2, and this meant that an array of capacitors had to be tested (see Experimental section for details). To ensure that the capacitors were able to sustain the electric field, each one in the array was individually confirmed to show a polarization hysteresis loop. Figure 3 is the resultant XRD patterns of the bilayer PZT thin film as a function of the applied DC bias (+ and −7 V). Figure 3a is the diffraction plot around the (001)/(100) peaks. Likewise, Figure 3b is for the (110)/(101) peak positions, and Figure 3c is a section of the diffraction pattern showing the (111) peak of the R layer. One finds that for the (001) and (111) peaks, very little change occurs as a function of applied bias. On the other hand, following positive bias application, there is significant increase in the (110) peak intensity as well as distinct changes in the peak shape. More importantly, we find that the peak returns to approximately the original shape and intensity values following subsequent negative-bias application.

If the films had undergone any electric-field induced transformation, distinct changes in the peak positions (and hence d-spacings) or intensities of the (001)/(100) and (111) peaks would be expected as the film would undergo significant lattice changes from a T to an R structure (or vice versa). The plots show that as a result of the field application there is a significant change in the ratios and peak shapes of only the (110)/(101) peaks, and the (001)/(100) and (111) peaks have remained relatively unperturbed. Thus, we conclude that the dominant mechanism is the occurrence of twin-boundary-motion (ferroelastic-domain-wall motion)-induced population redistribution of twin variants. We propose that upon electric-field application, in order to maintain energetically least expensive head-to-tail domain configurations, any change in the out-of-plane polarizations must be accompanied a concomitant change in the in-plane polarization. This entails that a ferroelectric switching is necessarily accompanied by a ferroelastic switching (identified as changes in the 110/101 variant fractions). In other words, it can create a very large surface displacement under the electric field and therefore can account for the observed high piezoelectric coefficient discussed below. This key experiment thus demonstrates that indeed upon application of an electric field, it is the change in the ferroelastic domains (non-180° domain switching) that dominates the electromechanical response, as opposed to a field-induced transformation into the R-phase. We also note here that the length scale of the XRD experiment (several square millimeters) is approximately six orders of magnitude larger than that of the local PFM studied area in Figure 2 (on the square-micrometer scale). In the present XRD experiment, given the relatively large sampling area, redistribution of variants occurred in such a way that only the average population ratio of (110)/(101)-oriented grains was affected.

To quantify the degree of electric-field-induced changes in the X-ray diffraction, the macroscopic strain comprised of both the microscopic lattice strain and the strain due to the ferroelastic domain switching (ε_f) has been calculated. From the changes in XRD peak position for the (110) peak before and after applying the electric field (Fig. 3b), the variation in *d*-spacing, and hence the microscopic lattice strain associated with these changes, was calculated as 0.00525. Then using the multiples of a random distribution (MRD) approach developed by Jones et al.,[31] the strain associated with the ferroelastic domain switching was

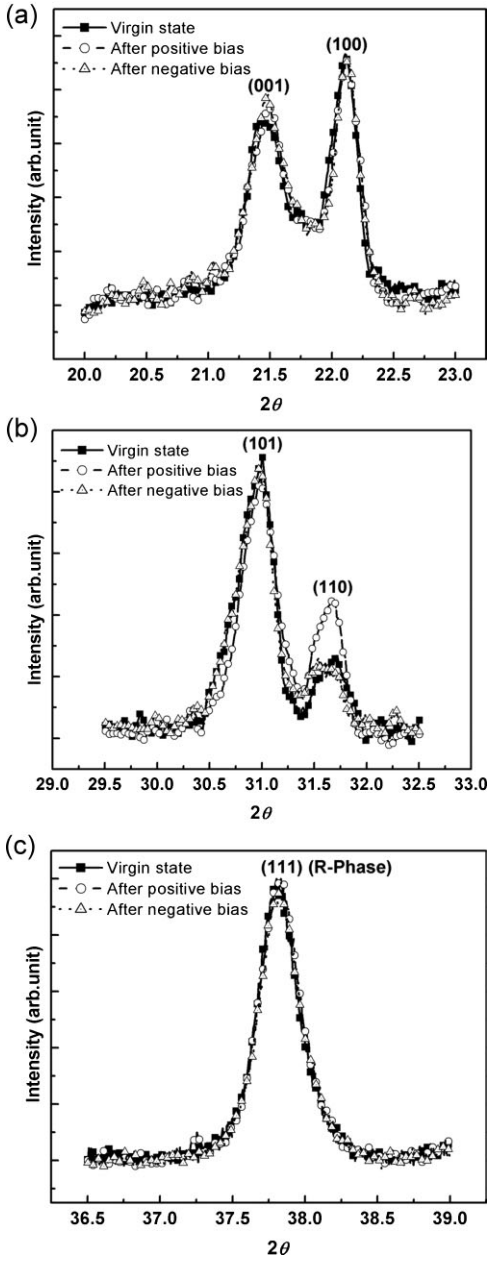

Figure 3. Electric-field dependent X-ray-diffraction pattern. Magnified XRD plots for the virgin structure and after applying positive and negative biases. a–c) T-phase (001)/(100), T-phase (101)/(110) and (111) R-phase peaks, respectively.

calculated. The degree of texture for the tetragonal (110) and (101) peak is given as[31]

$$MRD_{110} = 3\frac{I_{110}/I^R_{110}}{2(I_{101}/I^R_{101}) + (I_{110}/I^R_{110})} \quad (1)$$

where I_{110} and I_{101} are the integrated intensities of the (110) and (101) peaks, respectively, after applying the electric field. I^R_{110} and I^R_{101} are the intensities obtained for the bilayered thin film at its as-grown state. Thus, the electric-field-induced ferroelastic texture for these peaks is $MRD_{110} = 1.3691$, which also emphasizes the preferred orientation of the polar vector for (110) along the direction of the applied electric field. From MRD, the strain due to ferroelastic domain switching (ε_f) is calculated using the following expression[31]

$$\varepsilon_f = \frac{c-a}{a}\int_{\alpha=0}^{\alpha=\frac{\pi}{2}} [MRD_{110}(\alpha) - 1]\cos^2\alpha \sin\alpha . d\alpha \quad (2)$$

as 0.00536. In the above expression, c and a are the lattice parameters for $PbZr_{0.3}Ti_{0.7}O_3$ thin films, and α is the angle of rotation. Thus, the total strain associated with this ferroelastic-domain-wall motion is 0.0106 (that is, 212 pm V^{-1} for the 500 kV cm^{-1} applied electric field), which agrees with the PFM-measured piezoelectric coefficient value (effective d_{33}, Fig. 4a).

We also carried out quantitative PFM measurements on smaller capacitance pads to estimate the magnitude of this ferroelastic-domain-wall motion. The piezoelectric coefficient (effective d_{33}) of these thin films obtained via PFM is shown in Figure 4a. To avoid complications from an inhomogeneous field distribution often created by the AFM tip on a ferroelectric thin-film surface, all the quantitative measurements were performed on a top electrode (Pd) deposited on the ferroelectric surface. For comparison, we also plot in Figure 4a data for a standard PZT single layer of the same composition as the present top T layer. The bilayered thin film shows a piezoelectric constant of nearly 220 pm V^{-1}, which is three times larger than the constrained single-layered thin film. Also, the coercive field from the hysteresis loop for these bilayered thin films is of the same magnitude as the single layer, hence demonstrating significant potential in thin-film-based actuator applications using the present bilayer films. In the case of 90° (non-180°) domain-wall motion, it has been reported that the electro-mechanical parameter such as piezoelectric or dielectric coefficient is excited non-linearly by the AC amplitude.[20,32] Hence, a pertinent question is whether the giant piezoelectric coefficient observed in the bilayered thin film is an intrinsic or extrinsic behavior.

To answer this, we used AC-field-dependence analysis, where the piezoresponse of the bilayered thin films was measured as a function of AC amplitude using the lock-in amplifier, keeping the AC frequency constant without DC bias, to quantify the field dependence of the piezoelectric coefficients.[32,33] The first-, second-, and third-harmonic responses of the piezoresponse were captured and plotted against the AC amplitude (inset to Fig. 4a). The piezoresponse shows distinct nonlinear first-harmonic response, and particularly beyond the threshold AC amplitude (2.5 $V_{pk\text{-}pk}$), there is a rapid increase. This rapid nonlinear increase after the threshold field can be attributed to the drastic movement of the 90° domain wall.[32] In the case of second- and third-harmonic response, it shows negligible response confirming that the major contribution to the large piezoelectric response is from the 90°-domain-wall movement in these bilayered thin films. This also proves that the enhanced dielectric response observed for such bilayered systems[8,9] has a significant

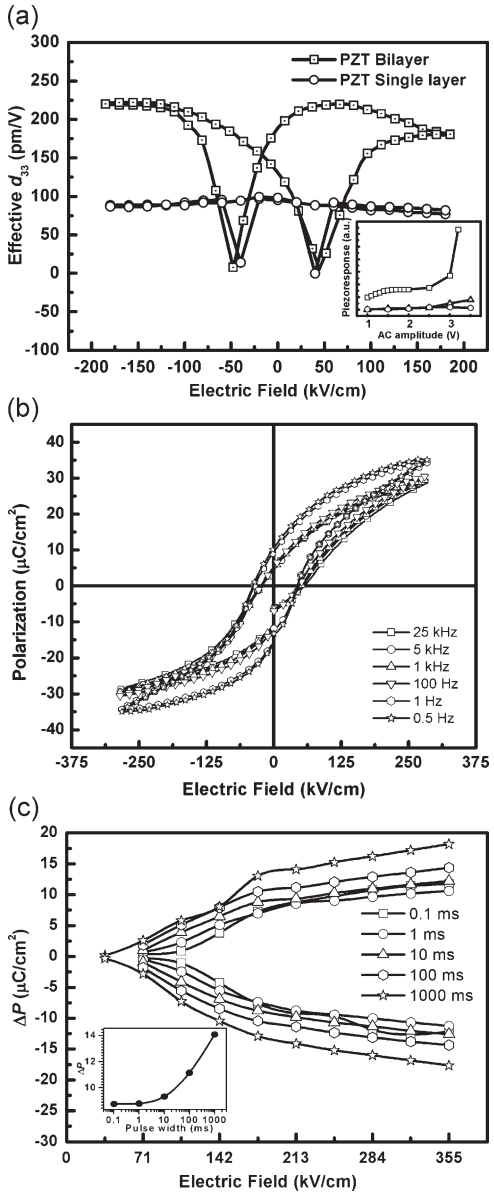

Figure 4. Piezoelectric and ferroelectric properties. a) Piezoelectric coefficient (effective) of the PZT bilayered thin films with AC-dependence plot as inset. The first-, second-, and third-harmonic responses are plotted with open squares, triangles, and circles, respectively. b) P–E hysteresis loop acquired for the bilayered thin films at a function of frequency from 25 kHz to 0.5 Hz. c) PUND measurements as a function of electric field and pulse width. Inset in c) is the pulse-width dependence of the switchable polarization at 213 kV cm^{-1}.

domain-wall-motion contribution and not solely space-charge-induced interface effects.

Finally, the ferroelectric hysteresis and positive-up negative-down (PUND) properties of this bilayered thin-film structure have also been investigated. Polarization-hysteresis loops for the bilayered PZT thin films captured as a function of frequency ranges from 25 kHz to 0.5 Hz are plotted in Figure 4b. The bilayered structure shows a remanent polarization (P_r) of ≈15 μC cm^{-2} at low frequencies. This low value is a reflection of the majority in-plane *a* domains that are present in the film. We find that as a function of frequency, there is a change in the value of the remanent polarization from ≈15 μC cm^{-2} (0.5Hz) to ≈7 μC cm^{-2} (25 kHz). To eliminate contributions from leakage and other non-switching components, PUND measurement was carried out using the same capacitance pad as a function of applied electric field (Fig. 4c) for different pulse widths. It also displays a rapid drop in the switched polarization (ΔP) with shorter pulse widths (the inset, which plots the ΔP at 213 kV cm^{-1}, shows that nearly 50% of ΔP is lost), signifying that for shorter pulse widths, the ferroelastic domains are too slow to respond to the applied field.

It is thus evident that the enhanced electromechanical coefficient measured in Figure 4a is a signature of increased ferroelastic-domain activity, particularly under relatively slow sweeping DC bias. An irreversible change would result in a large change in the P_r value, as was demonstrated on nanoscale ion-milled islands.[21] Instead, here these domains move reversibly instead of being completely eliminated in an irreversible manner after initial bias, and the reversibility may merely contribute to the increased hysteresis (widening of the P–E loop) rather than giant polarization. Notably, the same characteristic is also observed in the quantitative piezoelectric loops.

It can be shown in such a system that (details found elsewhere[34]) by applying the dense-domain model, the change of equilibrium volume fraction of *a* domains is obtained as

$$\Delta\beta_{multilayer} = \frac{(e_{c,T} - e_{a,T} + 2e^I_{ca,T} + e^I_{cR,T} - e^I_{aR,T})}{4e^I_{ca,T}} \quad (3)$$

where $e_{c,T}$ and $e_{a,T}$ are the elastic energies of the *c* and *a* domains at the interface plane in the tetragonal layer, $e^I_{ca,T}$ can be regarded as the indirect interaction energy between the *a* and *c* domains, and $\Delta\beta$ is the increase in the *a* domain volume fraction. The equation above is similar to previously derived forms for obtaining the change in the ferroelastic-domain fraction for a single-layer system,[25]

$$\Delta\beta_{singlelayer} = \frac{(e_{c,T} - e_{a,T} + e^I_{ca,T})}{2e^I_{ca,T}} \quad (4)$$

but it additionally contains two key terms, $e^I_{cR,T}$ and $e^I_{aR,T}$, as the interaction energies between *c* and *a* domains and the underlying rhombohedral film, respectively. Thus, we attribute the relatively large fraction of *a* domains for the bilayer system to the additional elastic-interaction-energy terms between the R and the T layer. Notably, there is a difference in the signs of $e^I_{aR,T}$ and $e^I_{cR,T}$, and this acts as a control mechanism to achieve the optimal domain volume fractions. Thus, interaction between the elastic self-strains of the T and R layers leads to a control parameter that can be easily tuned by changing the misfit strains at the T–R interface.

In summary, we demonstrate giant electromechanical coefficients in ferroelastically active bilayer ferroelectric thin-film systems. PFM coupled with electric-field dependent X-ray-diffraction experiments prove that the observed enhancement can be attributed to the presence of labile ferroelastic nanodomains in the top tetragonal layer, which show gross (reversible) movement under external electric fields.

Experimental

Bilayered thin-film structures consisting of a $PbZr_{0.3}Ti_{0.7}O_3$ (70 nm) deposited on top of a $PbZr_{0.7}Ti_{0.3}O_3$ (70 nm) were used in this study. The films were deposited by a multistep sol–gel route assisted by spin-coating on $Pt/Ti/SiO_2/Si$ substrates. X-Ray-diffraction measurements using Philips X-pert MRD verified that the structure of the PZT layers was polycrystalline with a preferential orientation along the (001)/(100) direction with small fraction of (111) orientation. Cross-sectional electron microscopy and electron-probe microanalysis confirmed that there was no intermixing between the functional layers. Further processing details and macroscopic ferroelectric properties are given elsewhere [35]. A multimode atomic force microscope with Pt/Ir-coated cantilever (with typical tip radius 7 nm, force constant 0.2 N m^{-1}, resonant frequency 13 kHz) was employed at a scan rate of 0.8 Hz for the visualization of domain structure. An AC signal $V_{ac} = V_o \sin(\omega t)$ with amplitude 1.5 V and frequency 7 kHz was applied between the AFM tip (movable top electrode) and the bottom electrode of the sample to acquire the piezoresponse images of the out-of -plane and in-plane components with the aid of two lock-in amplifiers. The as-grown (virgin) domain structure was visualized by monitoring the product of first harmonic amplitude and cosine of the phase, that is, the $(R \cdot \cos\theta)$ component, which is the real part, of the complex piezoresponse image. Then through the same AFM tip, DC bias was applied locally to a grain of interest. The d_{33} measurements and the Rayleigh analysis were performed using a custom-built circuit with the help of Stanford Research Systems' DDDA Data acquisition software. Nanotec's WsXM software was used to process and analyze the PFM images. For electric-field-dependent X-ray diffraction and functional-properties measurements, 100 nm thick 50 μm × 50 μm Pd top electrodes were photolithographically patterned as close as possible on top of the bilayered thin films. The typical gap between each pad was about 10 μm. The metal stage and a sample holder allows us to apply DC bias to each pad through an Agilent LCR meter, which aids us to confirm that the DC bias saturates the polarization, and thus the capacitor can sustain the applied electric field. X-ray diffraction patterns are then recorded using the Bruker D8 with Vantec detector. Ferroelectric hysteresis loops and PUND measurements were performed using a Radiant Premier II at room temperature. Cross-sectional TEM analysis were performed using a JEOL 3000F TEM operated at an accelerating voltage of 300 kV.

Acknowledgements

The work at UNSW was supported by NEDO, ARC Discovery Grant DP0666231 and LIEF LE0668257. V.A. acknowledges the ARC-ARNAM overseas travel award. F.K. and J.W. acknowledge the support of the Science and Engineering Research Council – A*Star, Singapore, under Grant No. 0521010047, and the National University of Singapore. The work at UMD was supported by NEDO, NSF MRSEC DMR 0520471 and ARO W911NF-071-1-0410. D.K. acknowledges the financial support from the Japan Society for the Promotion of Science. We are also thankful to L. Geske and Dr. M. Alexe for stimulating discussions. V.A. and D.K. contributed equally to this work. Supporting Information is available online from Wiley InterScience or from the author.

Received: December 15, 2008
Revised: February 18, 2009
Published online: April 20, 2009

[1] M. N. Baibich, J. M. Broto, A. Fert, F. N. Vandau, F. Petroff, P. Eitenne, G. Creuzet, A. Friederich, J. Chazelas, *Phys. Rev. Lett.* **1988**, *61*, 2472.
[2] S. S. P. Parkin, C. Kaiser, A. Panchula, P. M. Rice, B. Hughes, M. Samant, S. H. Yang, *Nat. Mater.* **2004**, *3*, 862.
[3] N. Reyren, S. Thiel, A. D. Caviglia, L. F. Kourkoutis, G. Hammerl, C. Richter, C. W. Schneider, T. Kopp, A. S. Ruetschi, D. Jaccard, M. Gabay, D. A. Muller, J. M. Triscone, J. Mannhart, *Science* **2007**, *317*, 1196.
[4] M. Dawber, N. Stucki, C. Lichtensteiger, S. Gariglio, P. Ghosez, J. M. Triscone, *Adv. Mater.* **2007**, *19*, 4153.
[5] H. N. Lee, H. M. Christen, M. F. Chisholm, C. M. Rouleau, D. H. Lowndes, *Nature* **2005**, *433*, 395.
[6] F. M. Pontes, E. Longo, E. R. Leite, J. A. Varela, *Appl. Phys. Lett.* **2004**, *84*, 5470.
[7] I. Vrejoiu, Y. Zhu, G. L. Rhun, M. A. Schubert, D. Hesse, M. Alexe, *Appl. Phys. Lett.* **2007**, *90*, 072909.
[8] C. Wang, Q. F. Fang, Z. G. Zhu, A. Q. Jiang, S. Y. Wang, B. L. Cheng, Z. H. Chen, *Appl. Phys. Lett.* **2003**, *82*, 2880.
[9] Z. H. Zhou, J. M. Xue, W. Z. Li, J. Wang, H. Zhu, J. M. Miao, *J. Appl. Phys.* **2004**, *96*, 5706.
[10] V. R. Cooper, K. Johnston, K. M. Rabe, *Phys. Rev. B* **2007**, *76*, 020103.
[11] C. Bungaro, K. M. Rabe, *Phys. Rev. B* **2004**, *69*, 184101.
[12] W. Tian, J. C. Jiang, X. Q. Pan, J. H. Haeni, Y. L. Li, L. Q. Chen, D. G. Schlom, J. B. Neaton, K. M. Rabe, Q. X. Jia, *Appl. Phys. Lett.* **2006**, *89*, 092905.
[13] A. L. Roytburd, S. Zhong, S. P. Alpay, *Appl. Phys. Lett.* **2005**, *87*, 092902.
[14] L. Geske, I. B. Misirlioglu, I. Vrejoiu, M. Alexe, D. Hesse, *J. Appl. Phys.* **2009**, *105*, 061607.
[15] K. Bhattacharya, R. D. James, *Science* **2005**, *307*, 53.
[16] E. Burcsu, G. Ravichandran, K. Bhattacharya, *Appl. Phys. Lett.* **2000**, *77*, 1698.
[17] C. S. Ganpule, V. Nagarajan, B. K. Hill, A. L. Roytburd, E. D. Williams, R. Ramesh, S. P. Alpay, A. Roelofs, R. Waser, L. M. Eng, *J. Appl. Phys.* **2002**, *91*, 1477.
[18] B. A. Tuttle, T. J. Headley, H. N. AlShareef, J. A. Voigt, M. Rodriguez, J. Michael, W. L. Warren, *J. Mater. Res.* **1996**, *11*, 2309.
[19] M. B. Kelman, P. C. McIntyre, B. C. Hendrix, S. M. Bilodeau, J. F. Roeder, *J. Appl. Phys.* **2003**, *93*, 9231.
[20] V. V. Shvartsman, N. A. Pertsev, J. M. Herrero, C. Zaldo, A. L. Kholkin, *J. Appl. Phys.* **2005**, *97*, 104105.
[21] V. Nagarajan, A. Roytburd, A. Stanishevsky, S. Prasertchoung, T. Zhao, L. Chen, J. Melngailis, O. Auciello, R. Ramesh, *Nat. Mater.* **2003**, *2*, 43.
[22] G. Le Rhun, I. Vrejoiu, L. Pintilie, D. Hesse, M. Alexe, U. Gosele, *Nanotechnology* **2006**, *17*, 3154.
[23] J. Ouyang, J. Slusker, I. Levin, D. M. Kim, C. B. Eom, R. Ramesh, A. L. Roytburd, *Adv. Funct. Mater.* **2007**, *17*, 2094.
[24] G. Arlt, *J. Mater. Sci.* **1990**, *25*, 2655.
[25] S. P. Alpay, A. L. Roytburd, *J. Appl. Phys.* **1998**, *83*, 4714.
[26] A. Schilling, R. M. Bowman, G. Catalan, J. F. Scott, J. M. Gregg, *Nano Lett.* **2007**, *7*, 3787.
[27] A. Roelofs, U. Bottger, R. Waser, F. Schlaphof, S. Trogisch, L. M. Eng, *Appl. Phys. Lett.* **2000**, *77*, 3444.
[28] S. V. Kalinin, B. J. Rodriguez, S. Jesse, J. Shin, A. P. Baddorf, P. Gupta, H. Jain, D. B. Williams, A. Gruverman, *Microsc. Microanal.* **2006**, *12*, 206.
[29] H. X. Fu, R. E. Cohen, *Nature* **2000**, *403*, 281.
[30] L. Bellaiche, A. Garcia, D. Vanderbilt, *Phys. Rev. B* **2001**, *6406*, 060103.
[31] a) J. L. Jones, E. B. Slamovich, K. J. Bowman, *J. Appl. Phys.* **2005**, *97*, 034113. b) T. S. Key, J. L. Jones, W. F. Shelley, B. J. Iverson, H. Y. Li, E. B. Slamovich, A. H. King, K. J. Bowman, *Mater. Sci. Forum* **2005**, *495–497*, 13.
[32] F. Xu, S. Trolier-McKinstry, W. Ren, B. Xu, Z. L. Xie, K. J. Hemker, *J. Appl. Phys.* **2001**, *89*, 1336.
[33] S. Trolier-McKinstry, N. B. Gharb, D. Damjanovic, *Appl. Phys. Lett.* **2006**, *88*, 202901.
[34] M. R. Mahjoub, V. Anbusathaiah, S. P. Alpay, V. Nagarajan, *J. Appl. Phys.* **2008**, *104*, 124103.
[35] F. C. Kartawidjaja, C. H. Sim, J. Wang, *J. Appl. Phys.* **2007**, *102*, 124102.